Hyperspectral Images Acquisition: an Efficient Capture and Processing Stitching Procedure for Medical Environments

Gonzalo Rosa*, Marta Villanueva*, Jaime Sancho*, Gemma Urbanos*, Luisa Ruiz*, Manuel Villa*, Alberto Martín*, Eduardo Juárez*, Luis Jiménez†, Miguel Chavarrías*, Alfonso Lagares†, César Sanz*
*Research Center on Software Technologies and Multimedia Systems. Universidad Politécnica de Madrid (UPM)
†Department of Neurosurgery, Hospital Universitario 12 de Octubre; Universidad Complutense de Madrid;
Instituto de Investigación Sanitaria Hospital 12 de Octubre (imas12), Madrid, España
{gonzalo.rosa.olmeda, manuel.villa.romero, a.martinp}@alumnos.upm.es
{marta.villanueva.torres, jaime.sancho, gemma.urbanos, luisa.rruiz, eduardo.juarez, miguel.chavarrias, cesar.sanz}@upm.es
{alfonsolagares, ljimenezr}@salud.madrid.org

***Abstract*—The complexity of the Hyperspectral (HS) imaging-based applications demands faster and more efficient acquisition and processing systems. Moreover, HSI technology is being more and more used within the medical imaging field, increasing and making more restrictive the requirements of the implementations. In this work, the authors present an efficient methodology for the acquisition and stitching processes when capturing line-scan based HS images. In order to verify the proposed methodology, a full hardware and software setup has been implemented. The proposed method has been tested scanning a reference polymer at different working distances and scroll speeds. The obtained results in laboratory show that the delta in PSNR keeps below 5% for all cases. Also, the correlation between comparable spectral signatures are not affected neither by the working distance nor by the acquisition speed.**

***Index Terms*—HSI, Medical, Imaging, Stitching, Hyperspectral**

I. Introduction

Since the very recent years, the Hyperspectral Imaging (HSI) technology has demonstrated its relevance among the under-expanding medical imaging diagnosis field. It has been successfully applied to such domains as skin tumor identification [1], ischemia detection during surgical procedures [2], brain tumor detection and, more precisely, delimitation of the tumor boundaries [3], among others. These solutions are presenting promising results [4] mainly founded on two pillars. First, the HSI technology is based on the existing relationship between materials and tissues and its response to a certain light spectrum range. In this way, each material can be characterized and thus differentiated from others, according to its light response, obtaining its spectral signature [5]. Secondly, the former description would require an unambiguous and independent analysis performed at pixel level [6]. Moreover, it would consider that each level represents only one type of material. To face with this problem, modelling procedures are applied considering Regions of Interest (RoIs) inside the registered pictures. To this end, powerful computing systems can be now used to accelerate Machine Learning (ML) algorithms [7] to help identifying different tissues and materials inside the picture.

Regarding medical imaging applications, HS cameras based on line-scan registration procedures are widely used [4]. However, due to its acquisition complexity and its low frame rate, snapshot cameras have been release more recently. These cameras solve the problems commented before, at the cost of lowering spatial and spectral resolutions. Nevertheless, commercial snapshot cameras are still strongly limited to a few dozens of spectral bands, whilst line-scan ones can capture hundreds or even thousand bands. Regarding the last ones, the camera should be scrolled along the scene in order to register it. This requires a scanning procedure during which the camera must stop at least for the minimum exposure time to take the picture before moving to the next point of capture. This scanning procedure must be performed as fast as possible due to constant scene changes because of eventual blood flooding in surgical procedures, heart-beating effects and other morphological processes [3].

In this work, a new procedure for the acquisition of HS images with line-scan cameras is presented. This procedure is targeted for its application on medical imaging-based systems in which the environment changes depending on the surgery procedures are a limiting key factor. Nevertheless, it could be easily applied to other application domains. The rest of the paper is organized as follows: Section 2 presents the background of the HSI technology and its acquisition basis. In Section 3, the proposed method for hyperspectral images is outlined. In Section 4, the test bench designed to verify the proposed method is described. In Section 5, the obtained results are

Remark: due to COVID-19 international situation since beginning 2020, some tests and results related with this work had to be performed in a laboratory instead of the targeted neurosurgery operating theater. This work was supported by the Regional Government of Madrid (Spain) through NEMESIS-3D-CM project (Y2018/BIO-4826).

978-1-7281-9132-4/20/$31.00 ©2020 IEEE

presented and discussed. Finally, Section 6 concludes the paper and presents our current work in progress.

II. Background

A. Line-scan HSI cameras on medical imaging

Over the past few years, HSI technology is being widely applied in different medical imaging research and new development projects. The field in which most focus is being made is on the delimitation of certain tissues during surgical interventions. Haliceck et al. presented in [7] how HSI technology combined with ML-based techniques can differentiate between tumor and healthy tissue. During the HELICoiD project [3], HSI technology was successfully applied to test the usefulness of the use of HSI for the detection of brain tumors. Zhi et al. applied this technology in the oncology field as well [8] to delineate tongue tumors, and Calin et al. [9] applied it for melanoma detection.

B. Line-scan HSI cameras acquisition basis

Line-scan HSI cameras (from this point linear HSI cameras) have a set of interference Fabry-Perot filters on top of the digital sensor which conforms the image as an array of rows belonging each one to an specific spectrum band. Each row that makes up the image captures only a limited number of pixels, so in order to capture an object the camera must move so that each row captures every point of the object. Once this scanning process is completed, the capture system has generated a certain number of images that need to be processed as part of the conformation of the final HSI cube. This procedure is called stitching and its objective is to create a HSI cube joining properly the rows present in the aforementioned captures. To this end, the algorithm selects all the slices of the current working band and from all the captures, shaping them all into the final image. This is exemplified in the Figure 1, here a five-pointed star represents the scene to be captured and four spectral bands are registered at once. First, the top point is captured at 400nm (A1) (Capture 1), then the camera is scrolled till Capture 2 point, here top point at 500nm (B1) and the two upper star-arms are registered at 400nm (A2). The procedure resumes by scrolling and capturing until the whole object has been fully, spatial and spectral, captured. Finally, stitching is applied: each capture is forked, reordered by spectral bands and joined conforming an HS cube, where the spatial dimensions are the width of the scene and the number of capture points multiplied by the number of spatial lines per capture whilst the z-axis represents the spectral bands. It is worth noting that there are also bands susceptible to be ignored; in Capture 1, 700nm, 600nm and 500nm bands have no information about the scene, therefore are completely useless. This process is extrapolated to every capture.

To perform the scanning accurately, there are a couple of parameters that need to be calculated previously. The first one is the vertical Field of View (FOV) in order to know the projected vertical distance covered by the plane. This parameter is calculated according to the Angular FOV (AFOV) and the Working Distance (W_d) in :

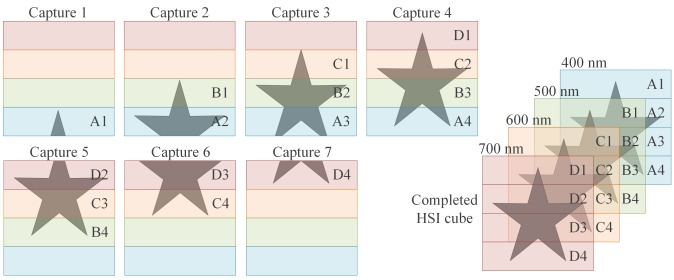

Fig. 1. Linear HSI acquisition procedure example for a HSI Cube conformed by 7 pictures and 4 spectral bands.

$$FOV = 2 \times W_d \times \tan(\frac{AFOV}{2}) \tag{1}$$

The AFOV is an angle which depends on the type of lens and the working distance is the length between the lens and the targeted object to be captured. The FOV is calculated following the Equation 1.

Hence, the total distance of the scrolling movement performed by the camera is defined as Room (R) and it is expressed in Equation 2, where L is the length of the object that it is going to be captured:

$$R = FOV + L \tag{2}$$

If R is longer than the actuator, the scanning cannot be ordered. Finally, the distance between captures defines the accuracy of the scanning: the camera must move a distance equivalent to the FOV of n pixels that make up a band. If the camera moves more than that, the result of the stitching is going to fail due to the overlapping between bands. Following, Equation 3 describes the calculation of this distance according to the FOV:

$$d = \frac{FOV \times P_b}{P_v} \tag{3}$$

Where P_b represents the number of pixels per band and P_v is the number of pixels that conforms the vertical component of the image.

III. Proposed method

In this section, the proposed method for linear HSI acquisition and stitching is outlined.

A. Calibration procedure

After acquiring the HS raw data, calibration is performed in order to obtain the reference reflectance ratio in the scene. To do so, white and dark references are captured. The white reference is acquired by taking a spectral image from a Reference Reflectance Target (RRT) in the same scene illumination conditions. This tile reflects constantly the 95% of the radiation over the wavelength range from $250\,nm$ to $2450\,nm$. The dimensions of the tile used are $20\,cm \times 20\,cm$. The dark reference is acquired by taking a spectral image with the camera lens covered. Then, the relative reflectance for the raw data is calculated following the Equation 4, where D

means the dark calibration image and W the white calibration image.

$$I = \frac{I_0 - D}{W - D} \times 100 \tag{4}$$

In order to validate the calibration results, a Reference Polymer – Diffuse Reflectance Standard can be used [10]. The polymer is a surface with constant reflection and certified calibration enabling an accurate validation.

B. Stitching method

Figure 2 represents, in a flowchart, the proposed method to perform the stitching while capturing images. When the scanning process begins, the system calculates the maximum number of captures ($M \times I$) that are going to be taken, the distance between each capture (defined in Equation 3) and the time needed to perform the scan. Therefore, the process will end when the number of captures reaches the calculated maximum. If the number of captures taken is less than the maximum, the following occurs:

1) The linear actuator moves the camera the distance calculated in Equation 3 and the system orders the HSI camera to take a capture.
2) Once the capture has been taken, there are three possible options to stitch that image:
   - If the number of images taken (NbI) is less than or equal to the number of total bands (Tb) the number of bands with information is increasing , which means that it is the first phase of the scan (Figure 1 captures 1, 2, 3). This condition occurs because the object is entering the image from below, meaning that the upper bands have no useful information.
   - If the number of images is greater than $M \times I$ minus the total number of band, the number of visible bands is decreasing, meaning that it is the last phase of the scan (Figure 1 captures 5, 6, 7). This condition is the opposite to the previous one: the lower bands have no useful information because the object is disappearing through the upper bands.
   - If neither of the above conditions are true, it means that all bands have information to capture and, as a consequence, the system is in the intermediate phase of the scanning (Figure 1 capture 4). In this condition every single band have useful information.
3) Once each frame has been successfully processed, it is saved and the counter is increased by one. Then, the systems resumes from the first step.

This three-condition algorithm is implemented to exclude, in real time, the bands with no useful information. The algorithm presented here is much more effective than the intuitive way of doing it, which would be to capture all the bands from all the captures and then eliminate them in post-processing. Therefore,

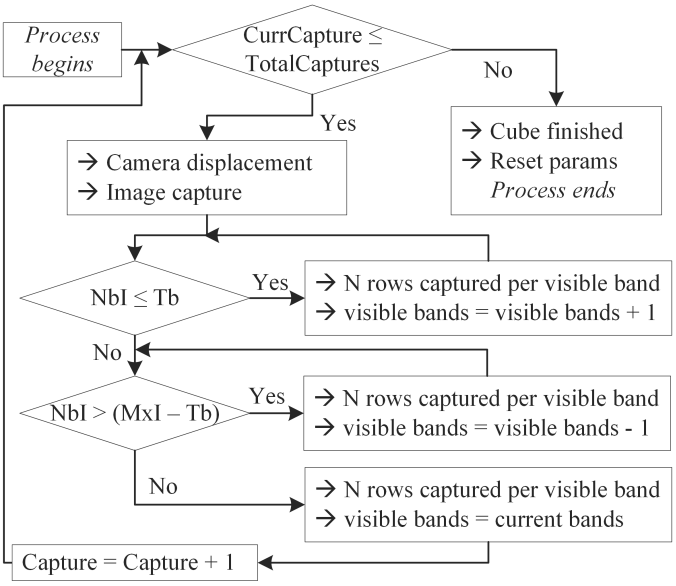

Fig. 2. Flowchart representing the HS Cube construction applying the proposed stitching method.

C. Implementation

The capture system has been developed in Python and it is composed of two modules coordinated with each other: the actuator control system, which controls the accuracy and precision of the movements that the actuator has to execute and the camera control systems that implements the functionalities needed to capture. For processing the images files, the OpenCV library [11] has been used along with the NumPy [12] module. It is worth noting that all stitching applicable parameters are currently offline pre-calculated.

IV. Test bench

The proposed method has been tested using a full-featured capture system. Figure 4 illustrates this setup integrated by the following items:

- One linear HSI camera [13] (C_a). Its main features are summarized in Table I.
- The linear camera has been mounted over the moving platen of an actuator system [14], whose main features are listed in Table II. Room (R) parameter previously defined in Equation 2 is here represented.
- Both item are mounted over an extensible arm attached to an adjustable height base, allowing to modify the Working distance (W_d) parameter, already presented in Equation 3.
- Under the actuator, an scenario composed by a millimeter ruler and a HS reference polymer is presented for its capture. The reference polymer is an optical gadget whose spectral signature is provided by its manufacturer.

The setup also includes a workstation running the control software for cameras and actuator, a laser rangefinder to measure more precisely W_d and a 150W light source [15]. The light beam has been directed using fiber optic cables placed on

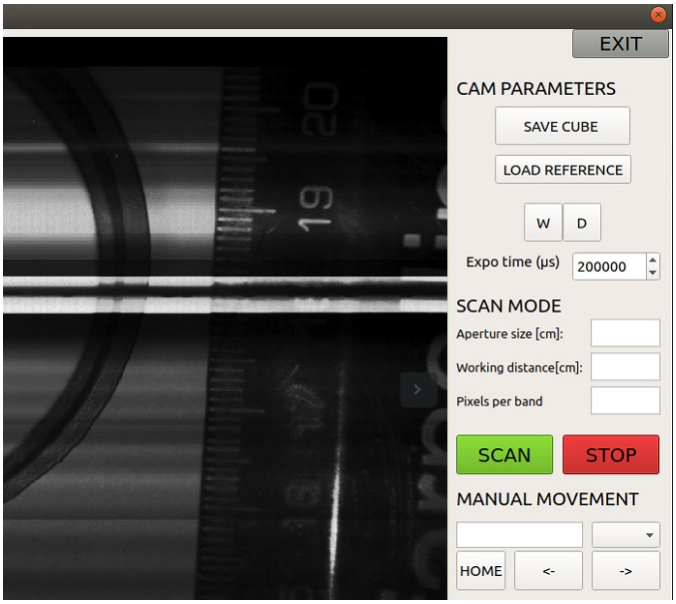

Fig. 3. Appearance of the configurable parameters of the controlling interface (camera and actuator).

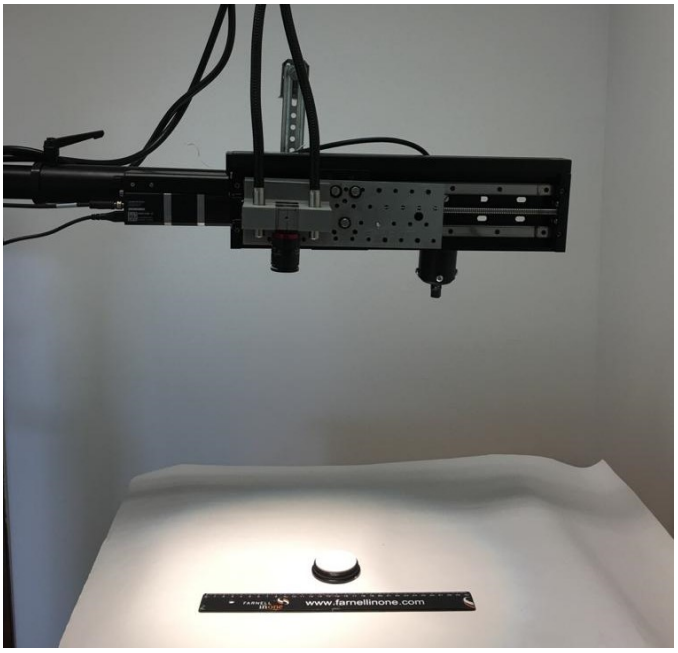

Fig. 4. Picture of the designed setup, including camera, actuator, ruler and polymer.

both sides of the C_a camera. Parameter settings is done by the interface showed in Figure 3. It is possible to adjust the starting position of the actuator, set the exposure time according to the light environment, order a scanning stop and set the main parameters as working distance and the size of the scene.

V. Results and Discussion

Aspects such as working distance or surgical incision size are not easily controlled inside the operating room. In addition, blood flooding or heart-beating, among others, are factors which can contribute to increase acquisition times and, therefore, degrade the quality of captured images. In order to verify the feasibility of our system in an operating room, six different scenarios have been prepared by modifying the working distance and actuator speed. The working distance has been set from $40\,cm$ to $60\,cm$, where $40\,cm$ is the minimum safety distance and $60\,cm$ is the maximum distance the RRT reflected energy can be captured from the camera. Likewise, the actuator speed has been set from $30\,mm/s$ to $100\,mm/s$. The experiments involve capturing the light reflected from a calibrated polymer placed next to a ruler with a linear HSI camera docked on the linear actuator as shown in Figure 5. Then, these scenarios have been compared using the Peak Signal-to-Noise Ratio (PSNR) and the Structural Similarity (SSIM) metrics. For each working distance series, the values taken at $30\,mm/s$ have been selected as references . Results are included in Table III.

TABLE I
Main features of the Linear HSI camera

Parameter	Value
Sensor	CMOSIS CMV2000
Spacial resolution	2048×1088 — $2.2\,Mpx$
Spectral range	$470 - 900\,nm$
Bands	216 bands: 64 VIS — 128 NIR
Optic	$35\,mm$ — AFOV $= 9.8°$

TABLE II
Main features of the high precision actuator

Parameter	Value
Default resolution	$0.1953125\,\mu m$
Travel range	$300\,mm$
Accuracy	$13\,\mu m$
Maximum speed	$100\,mm/s$
Encoder type	Linear quadrature

TABLE III
PSNR and SSIM obtained for different distances and actuator speeds.

Metrics	Distance (in cm)	Speed (in mm/s)	
		70	100
PSNR (in dB)	40	39.0377	35.5031
	50	40.4606	39.7789
	60	40.8827	40.3076
SSIM index	40	0.7926	0.7768
	50	0.9673	0.9673
	60	0.9705	0.9685

Results show that increasing the working distance and actuator speed does not spoil the quality of the resulting HS cubes. On the one hand, the delta PSNR obtained between captures is under 1% for the $50\,cm$ and $60\,cm$ scenes, and

under 5% for the $40\,cm$ scene. It should be noted that the greatest errors are located in shinny areas and borderlines, as shown in Figure 6. On the other hand, the SSIM obtained shows high similarity between the structures in the scene, proving that the HS cubes are similarly reconstructed along the different actuator speeds.

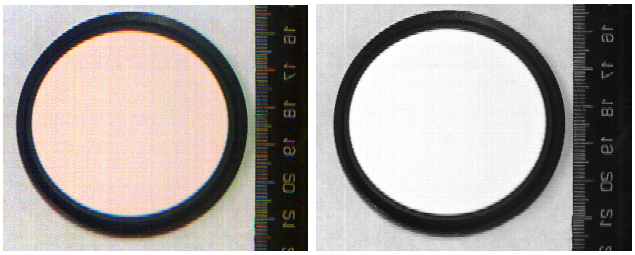

Fig. 5. Captures of the polymer used as reference: RGB reconstruction of the HSI cube (left) and capture of the 580 nm band (right).

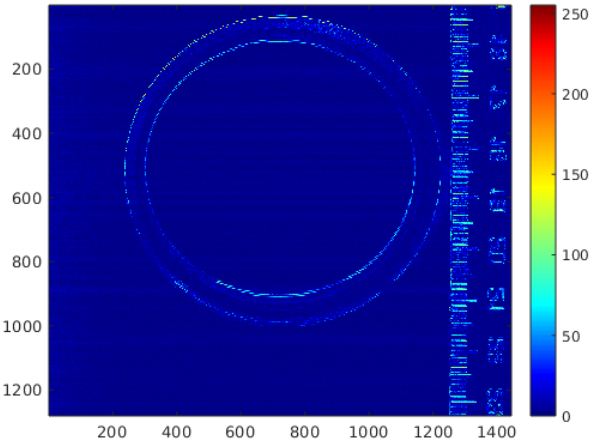

Fig. 6. Differences between captures performed from $40\,cm$ distance at $100\,mm/s$ and at $30\,mm/s$.

Additionally, the spectral signature of the captured polymer has been studied by computing the correlation between the different spectral signatures captured and the calibrated polymer signature. These results are summarized in Table IV.

Firstly, considering the correlation between the captured spectrum and the calibrated spectrum, it is observed that the quality of the HS cube remains similar for all the tested scenes. However, in the comparison between the reference image and the scene, the correlation result shows differences between the captured spectrum. These results are consequence of the different illumination conditions of each scene and eventual reflections caused by spurious glitters. Particularly, the scene capture at $50\,cm$ have the worst performance as a result of its calibration step. As it is observed in Figure 7, the reflectance for this scene goes over 100% which indicates that the white reference used during calibration had lower reflectance than the actual scene.

Overall, these results show that the quality of the spectrum remains the same while increasing the actuator speed and/or changing the working distance. However, differences arise due to differing illumination conditions. Light intensity can change when increasing or decreasing the working distance, further research should be conducted on how to control these changes and how it affects to the final result quality.

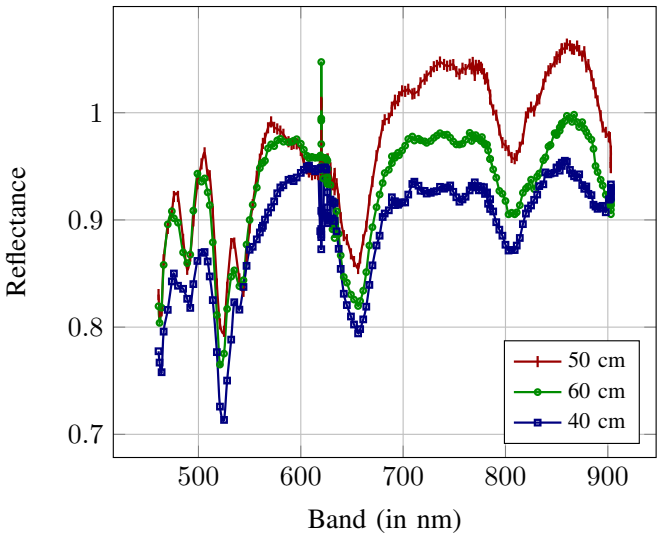

Fig. 7. Reflectances captured at 100mm/s with a distance of 40cm, 50cm and 60cm.

TABLE IV
CORRELATIONS OBTAINED FROM THE CAPTURES TAKEN AT DIFFERENT DISTANCES AND SPEEDS

Correlations	Distance (in cm)	Speed (in mm/s)		
		30	70	100
Reference image vs. rest of images	40	1.00000	0,99279	0,95246
	50	0.59228	0,62180	0,66428
	60	0.82358	0,81158	0,80600
Reference spectrum vs. obtained spectrum	40	0,82904	0,84857	0,91573
	50	0,81676	0,81420	0,84343
	60	0,88674	0,88023	0,90997

VI. CONCLUSIONS AND FUTURE WORK

HSI technology is increasingly being used in the field of medical imaging, and more specifically its application to differentiate between health and tumor tissues. In this paper, an efficient procedure for the HS linear-images acquisition and stitching is presented. Up to the best of our knowledge, this is the first detailed description in the scientific literature about this methods applied on the HSI stitching process for medical imaging, therefore no comparison can be made between other methodologies. The proposed method has been implemented over a full setup combined by hardware and software. The results show how the system response, in terms of both, PSNR and spectrum correlation, remains stable when varying the capture speed or working distance.

Due to the COVID-19 international situation since begging 2020, and specially the applied quarantine and confinement measures, both, test bench and results, had to be dramatically restricted to laboratory verification. Hence, in the future, authors would extend the verification process to a neurosurgery operating theater. In this sense, it is worth nothing that greater working distances will need larger RRT.

Additionally, authors will continue working on the improvement of the implemented solution. Specifically, work is underway to parallelize the HSI processing and capture procedure as well as to pursue the eventual updating of stitching data in real time.

REFERENCES

[1] L. A. Zherdeva, I. A. Bratchenko, O. O. Myakinin, A. A. Moryatov, S. V. Kozlov, and V. P. Zakharov, "In vivo hyperspectral imaging and differentiation of skin cancer," vol. 10024, pp. 658 – 665, 2016. [Online]. Available: https://doi.org/10.1117/12.2246433

[2] H. Akbari, Y. Kosugi, K. Kojima, and N. Tanaka, "Detection and analysis of the intestinal ischemia using visible and invisible hyperspectral imaging," *IEEE Transactions on Biomedical Engineering*, vol. 57, no. 8, pp. 2011–2017, 2010.

[3] H. Fabelo, S. Ortega, S. Kabwama, G. M. Callico, D. Bulters, A. Szolna, J. F. Pineiro, and R. Sarmiento, "HELICoiD project: a new use of hyperspectral imaging for brain cancer detection in real-time during neurosurgical operations," vol. 9860, pp. 1 – 12, 2016. [Online]. Available: https://doi.org/10.1117/12.2223075

[4] G. Lu and B. Fei, "Medical hyperspectral imaging: a review," *Journal of Biomedical Optics*, vol. 19, no. 1, pp. 1 – 24, 2014. [Online]. Available: https://doi.org/10.1117/1.JBO.19.1.010901

[5] S. L. Jacques, "Optical properties of biological tissues: a review," *Physics in Medicine and Biology*, vol. 58, no. 11, pp. R37–R61, may 2013. [Online]. Available: https://doi.org/10.1088/0031-9155/58/11/r37

[6] R. Pourreza, F. Saki, N. Kehtarnavaz, P. Leboulluec, and H. Liu, "Classification of ex-vivo breast cancer positive margins measured by hyperspectral imaging," *2013 IEEE International Conference on Image Processing, ICIP 2013 - Proceedings*, 09 2013.

[7] M. Halicek, G. Lu, J. V. Little, X. Wang, M. Patel, C. C. Griffith, M. W. El-Deiry, A. Y. Chen, and B. Fei, "Deep convolutional neural networks for classifying head and neck cancer using hyperspectral imaging," *Journal of Biomedical Optics*, vol. 22, no. 6, pp. 1 – 4, 2017. [Online]. Available: https://doi.org/10.1117/1.JBO.22.6.060503

[8] L. Zhi, D. Zhang, J. Q. Yan, Q. L. Li, and Q. L. Tang, "Classification of hyperspectral medical tongue images for tongue diagnosis," *Computerized medical imaging and graphics : the official journal of the Computerized Medical Imaging Society*, vol. 31, pp. 672–8, 01 2008.

[9] M. Calin, S. Parasca, D. Savastru, and D. Manea, "Hyperspectral imaging in the medical field: Present and future," *Applied Spectroscopy Reviews*, vol. 49, 08 2014.

[10] S. Optics, "Zenith litetm targets," url: http://sphereoptics.de/en/wp-content/uploads/sites/3/2014/03/SphereOptics-Ultralight-Targets-Zenith-Lite.pdf.

[11] OpenCV. OpenCV. [Online]. Available: https://opencv.org/

[12] Python. NumPy. [Online]. Available: https://numpy.org/

[13] L. camera model, "MQ022HG-IM-LS150-VISNIR." [Online]. Available: https://www.ximea.com/en/products/hyperspectral-cameras-based-on-usb3-xispec/mq022hg-im-ls150-visnir

[14] A. device. X-LRQ-DE Series User's Manual. [Online]. Available: https://www.zaber.com/manuals/X-LRQ-DE

[15] Fiber-lite. Model Mi-LED: LED Fiber Optic Illuminator. [Online]. Available: https://www.setra.com/hubfs/mi-led-data-sheet.pdf